μOCT imaging using depth of focus extension by self-imaging wavefront division in a common-path fiber optic probe

Biwei Yin,[1] Kengyeh K. Chu,[1] Chia-Pin Liang,[1] Kanwarpal Singh,[1] Rohith Reddy,[1] and Guillermo J. Tearney[1,2,3,*]

[1]*Wellman Center for Photomedicine, Harvard Medical School and Massachusetts General Hospital, 55 Fruit Street, Boston, MA 02114, USA*

[2]*Harvard-MIT Division of Health Sciences and Technology, 77 Massachusetts Avenue, Cambridge, MA 02139, USA*

[3]*Department of Pathology, Harvard Medical School and Massachusetts General Hospital, 55 Fruit Street, Boston, MA 02114, USA*

[*]*gtearney@partners.org*

Abstract: Optical coherence tomography (OCT) is an attractive medical modality due to its ability to acquire high-resolution, cross-sectional images inside the body using flexible, small-diameter, scanning fiber optic probes. Conventional, cross-sectional OCT imaging technologies have approximately 10-μm axial resolution and 30-μm lateral resolution, specifications that enable the visualization of microscopic architectural morphology. While this resolution is useful for many clinical applications, it is insufficient for resolving individual cells that characterize many diseases. To address this gap, a supercontinuum-laser-based, μm-resolution OCT (μOCT) system and a 500 μm-diameter, extended depth of focus single fiber optic probe for endoscopic and intravascular imaging were designed and fabricated. At the distal tip of the fiber optic probe, a cylindrical waveguide was used to divide the wavefront to provide multiple circular propagation modes. Once transmitted through a relatively high NA lens (NA >0.1), these modes were projected as multiple coaxial foci (~3 μm full width at half maximum (FWHM)) over a greatly extended focal depth range. The distal tip of the probe also contained a common-path reference reflectance to minimize polarization and dispersion imbalances between sample and reference arm light. Measurements showed that the probe provides a 20-fold depth of focus extension, maintaining a 3-5 μm lateral resolution (FWHM of PSF) and a 2 μm axial resolution over a depth range of approximately 1 mm. These results suggest that this new optical configuration will be useful for achieving high-resolution, cross-sectional OCT imaging in catheter/endoscope-based medical imaging devices.

OCIS codes: (050.1220) Apertures; (070.7345) Wave propagation; (080.2740) Geometric optical design; (120.4640) Optical instruments; (170.2150) Endoscopic imaging; (170.4500) Optical coherence tomography.

References and links

1. D. Huang, E. A. Swanson, C. P. Lin, J. S. Schuman, W. G. Stinson, W. Chang, M. R. Hee, T. Flotte, K. Gregory, C. A. Puliafito, and J. G. Fujimoto, "Optical coherence tomography," Science **254**(5035), 1178–1181 (1991).
2. G. J. Tearney, M. E. Brezinski, B. E. Bouma, S. A. Boppart, C. Pitris, J. F. Southern, and J. G. Fujimoto, "In Vivo endoscopic optical biopsy with optical coherence tomography," Science **276**(5321), 2037–2039 (1997).
3. M. E. Brezinski, G. J. Tearney, B. E. Bouma, S. A. Boppart, M. R. Hee, E. A. Swanson, J. F. Southern, and J. G. Fujimoto, "Imaging of coronary artery microstructure (in vitro) with optical coherence tomography," Am. J. Cardiol. **77**(1), 92–93 (1996).
4. L. Liu, J. A. Gardecki, S. K. Nadkarni, J. D. Toussaint, Y. Yagi, B. E. Bouma, and G. J. Tearney, "Imaging the subcellular structure of human coronary atherosclerosis using micro-optical coherence tomography," Nat. Med. **17**(8), 1010–1014 (2011).
5. W. Drexler, "Ultrahigh-resolution optical coherence tomography," J. Biomed. Opt. **9**(1), 47–74 (2004).

#258710 Received 2 Feb 2016; revised 29 Feb 2016; accepted 1 Mar 2016; published 4 Mar 2016

6. A. R. Tumlinson, J. K. Barton, B. Povazay, H. Sattman, A. Unterhuber, R. A. Leitgeb, and W. Drexler, "Endoscope-tip interferometer for ultrahigh resolution frequency domain optical coherence tomography in mouse colon," Opt. Express **14**(5), 1878–1887 (2006).
7. R. A. Leitgeb, M. Villiger, A. H. Bachmann, L. Steinmann, and T. Lasser, "Extended focus depth for Fourier domain optical coherence microscopy," Opt. Lett. **31**(16), 2450–2452 (2006).
8. D. Lorenser, C. Christian Singe, A. Curatolo, and D. D. Sampson, "Energy-efficient low-Fresnel-number Bessel beams and their application in optical coherence tomography," Opt. Lett. **39**(3), 548–551 (2014).
9. K. M. Tan, M. Mazilu, T. H. Chow, W. M. Lee, K. Taguichi, B. K. Ng, W. Sibbett, C. S. Herrington, C. T. A. Brown, and K. Dholakia, "In-fiber common-path optical coherence tomography using a conical-tip fiber," Opt. Express **17**(4), 2375–2384 (2009).
10. J. Xing, J. Kim, and H. Yoo, "Design and fabrication of an optical probe with a phase filter for extended depth of focus," Opt. Express **24**(2), 1037–1044 (2016).
11. B. A. Standish, K. K. C. Lee, A. Mariampillai, N. R. Munce, M. K. K. Leung, V. X. D. Yang, and I. A. Vitkin, "In vivo endoscopic multi-beam optical coherence tomography," Phys. Med. Biol. **55**(3), 615–622 (2010).
12. D. Lorenser, X. Yang, and D. D. Sampson, "Ultrathin fiber probes with extended depth of focus for optical coherence tomography," Opt. Lett. **37**(10), 1616–1618 (2012).
13. T. S. Ralston, D. L. Marks, P. S. Carney, and S. A. Boppart, "Interferometric synthetic aperture microscopy," Nat. Phys. **3**(2), 129–134 (2007).
14. J. Mo, M. de Groot, and J. F. de Boer, "Focus-extension by depth-encoded synthetic aperture in Optical Coherence Tomography," Opt. Express **21**(8), 10048–10061 (2013).
15. A. Kumar, W. Drexler, and R. A. Leitgeb, "Subaperture correlation based digital adaptive optics for full field optical coherence tomography," Opt. Express **21**(9), 10850–10866 (2013).
16. R. Ulrich and G. Ankele, "Self-imaging in homogeneous planar optical waveguides," Appl. Phys. Lett. **27**(6), 337–339 (1975).
17. O. Bryngdahl and W. H. Lee, "On light distribution in optical waveguides," J. Opt. Soc. Am. **68**(3), 310–315 (1978).
18. S. W. Allison and G. T. Gillies, "Observations of and applications for self-imaging in optical fibers," Appl. Opt. **33**(10), 1802–1805 (1994).
19. X. Zhu, A. Schülzgen, H. Wei, K. Kieu, and N. Peyghambarian, "White light Bessel-like beams generated by miniature all-fiber device," Opt. Express **19**(12), 11365–11374 (2011).
20. B. Yin, J. Dwelle, B. Wang, T. Wang, M. D. Feldman, H. G. Rylander 3rd, and T. E. Milner, "Fourier optics analysis of phase-mask-based path-length-multiplexed optical coherence tomography," J. Opt. Soc. Am. A **32**(11), 2169–2177 (2015).
21. R. K. Wang, "In vivo full range complex Fourier domain optical coherence tomography," Appl. Phys. Lett. **90**(5), 054103 (2007).
22. W. C. Kuo, C. M. Lai, Y. S. Huang, C. Y. Chang, and Y. M. Kuo, "Balanced detection for spectral domain optical coherence tomography," Opt. Express **21**(16), 19280–19291 (2013).
23. T. Wang, W. Wieser, G. Springeling, R. Beurskens, C. T. Lancee, T. Pfeiffer, A. F. W. van der Steen, R. Huber, and G. Soest, "Intravascular optical coherence tomography imaging at 3200 frames per second," Opt. Lett. **38**(10), 1715–1717 (2013).

1. Introduction

Optical coherence tomography (OCT) [1, 2] is an interferometric coherence ranging-imaging modality that has significantly better resolution than other clinical imaging techniques such as ultrasound, computed tomography (CT), and magnetic resonance imaging (MRI). Key features of OCT include cross-sectional imaging, which is important clinically because many diseases manifest below the tissue surface, and its capability to image inside the body using flexible, small-diameter, fiber optic probes. While conventional OCT with 10-μm axial resolution and 30-μm lateral resolution can provide important diagnostic architectural morphologic information [3], disease is fundamentally caused by cellular and sub-cellular processes that cannot be seen at these resolutions. As a result, there has been great interest in improving the resolution of OCT by an order of magnitude along each dimension to enable visualization of abnormal cells in living patients [4]. Near-isotropic μm-resolution forms of OCT have been termed ultra-high-resolution OCT (UHR-OCT) or μOCT in literatures [4–6].

With the introduction of single-mode-ultra-broad bandwidth supercontinuum light sources, significant progress has been made towards increasing the axial resolution of OCT, and recent studies using supercontinuum sources and common path interferometer configurations have shown μOCT axial resolutions ranging from 1 to 2 μm in tissue [4]. The lateral resolution of OCT is determined by the spot size in the sample, governed by the numerical aperture (NA) of the sample arm's focusing optics. Using conventional optics, it has been difficult to improve lateral resolution beyond approximately 30 μm without

#258710 Received 2 Feb 2016; revised 29 Feb 2016; accepted 1 Mar 2016; published 4 Mar 2016

sacrificing cross-sectional imaging because depth of focus (DOF) is proportional to the square of the lateral spot size.

Various approaches have been proposed to extend the DOF of OCT sample arm optics, such as Bessel beam optics [7–9], aperture apodization [4, 10], multi-focus sample arm optics [11, 12], and numerical refocusing [13–15]. A Bessel beam is usually created by using an axicon lens in the sample arm instead of a conventional objective [7–9]. Aperture apodization shapes the beam profile by modifying the amplitude and/or phase of the light transmitted through the sample arm optics' pupil [4, 10]. Both methods suffer from poor signal collection efficiency, side-lobe artifacts, and difficulty in alignment and miniaturization. Multi-beam multi-focus techniques [11] apply a series of beams to acquire in-focus images at different depth regions of the sample. These sub-images are then combined to achieve one final image that has a DOF that is proportional to the number of sub-images applied in the system. These techniques substantially increase system, probe, and image reconstruction complexity. A single-beam dual-focus fiber optic probe has been reported, but the design of the probe could make it difficult to further extend the DOF beyond the demonstrated factor of 1.55 [12]. Numerical refocusing methods include interferometric synthetic aperture microscopy (ISAM) [13], synthetic aperture [14] and subaperture [15] defocus correction. These techniques require multiple image acquisitions, computationally intensive processing and phase stability during data acquisition.

As of yet, most of these solutions either do not extend the focus sufficiently or are too large or complex to fit within the confines of small diameter scanning probes intended to be inserted inside the body. To address this technical barrier, we developed a single-fiber self-imaging wavefront division probe that has a diameter of 500 μm, less than 4-mm rigid length, and a 20-fold DOF extension compared to a conventionally focused beam with comparable lateral resolution. The capability of this probe to maintain a tightly focused spot over a large distance is critical for enabling *in-vivo* internal organ cross-sectional μOCT imaging at the cellular level.

2. Method

2.1 Self-imaging wavefront division fiber optic probe

Figure 1(a) shows a schematic of the extended DOF μOCT probe. A circularly cylindrical waveguide is placed at the output of a single-mode fiber (SMF). The waveguide wall reflects the SMF output light an angle-dependent number of times, creating multiple coaxial propagation modes [16–19]. Each mode diverges within the glass spacer and is focused by a lens to a mode-dependent focal depth. Each high order mode, representing at least one reflection from the waveguide's wall, can be considered as originating from the mirror image of the input point source (core of the SMF), such that the superimposed field divides the aperture wavefront into multiple annular zones. We therefore call this imaging arrangement a self-imaging wavefront division optical system.

A simulation based on Fresnel diffraction shows that this optical system generates multiple on-axis foci from one single original beam (Fig. 1(b) and 1(c)). Figures 1(b) and 1(c) depict the simulated field intensity distribution at a wavelength of 800 nm for a fiber probe that consists of an SMF with an NA of 0.13 at a wavelength of 630 nm (630HP, Nufern, CT, USA), a circularly cylindrical 50 μm diameter waveguide (FG050UGA, Thorlabs Inc., NJ, USA), that spans 1.2 mm, a spacer with a length of 1.6 mm, a GRIN lens (GT-LFRL-050, GRINTECH GmbH, Germany) with a focal length of approximately 0.5 mm, and a BK-7 right-angle prism with a leg length of 300 μm (66-770, Edmund Optics Inc., NJ, USA). The refractive index of the medium in image space is assumed to be 1.34. As shown in the simulation, 3-4 major foci are introduced in the image space. These foci maintain a lateral resolution of better than 5 μm over a 1 mm depth range. Another feature of this configuration is that the mode with the highest intensity (1st order mode, labeled in Fig. 1(c)) is positioned in the middle of the extended focus range, potentially compensating for attenuation that may be encountered when the beam propagates through tissue. In between the focused modes, a

#258710 Received 2 Feb 2016; revised 29 Feb 2016; accepted 1 Mar 2016; published 4 Mar 2016

few intensity gaps can be seen along the Z-axis. The widths of these gaps are small for this particular configuration; the on-axis intensity remains above 50% of the peak intensity of each major mode for greater than 80% of the 1 mm depth range. Axial interference between the 0th order mode and the high order modes takes place in 0th order mode focusing region due to the extension of high order modes' foci. Therefore the 0th order mode focus is slightly different from that of a conventional Gaussian beam's focus. In addition to creating additional foci, modes of order higher than 0th provide an individually extended DOF compared to a standard Gaussian beam as their pseudo-Bessel beam property.

In addition to providing a highly extended DOF, the distal end of the probe contains a prism that redirects the sample arm light in a direction that is nearly perpendicular to the optical axis. The distal face of this prism also serves as a common path reference reflector that minimizes sample-reference arm polarization and/or dispersion imbalances that would otherwise prohibit high axial resolution OCT imaging [9].

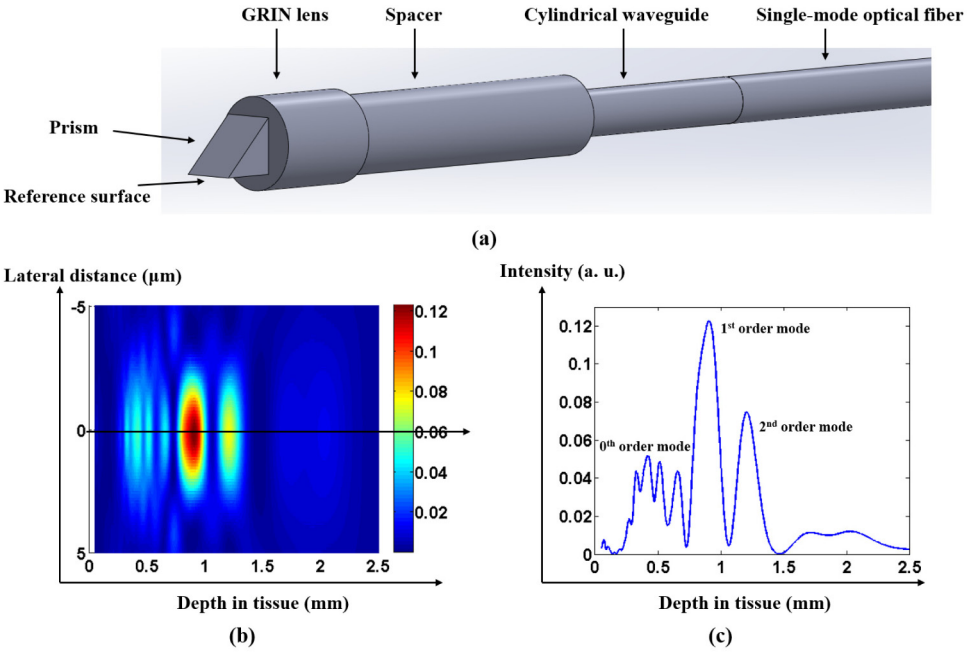

Fig. 1. (a) A self-imaging wavefront division fiber optic probe design consisting of a circularly cylindrical waveguide, a glass spacer, a GRIN lens and a right-angle prism. A common-path configuration is achieved by using the back-reflection from the prism-air interface as the OCT reference. (b) Simulated intensity distribution in image space, color bar intensity is in linear scale with arbitrary units (a. u.). (c) Simulated on-axis intensity distribution.

2.2 μOCT system

The μOCT system is a common-path spectral-domain OCT (SD-OCT) system that uses a supercontinuum laser as the light source (SuperK Extreme OCT, NKT Photonics, Denmark). Spectral interferometric detection is accomplished by a broadband (650-950 nm) spectrometer consisting of a grating, custom-designed focusing optics, and a line-scan camera (SPL8192, Basler, Germany) operating at a maximum 38 kHz A-line rate (24 μs integration time). The μOCT system's peak sensitivity (with wavefront division fiber optic probe as sample arm) is 88 dB and the 6 dB sensitivity roll-off occurs at a depth of 1.5 mm in air.

2.3 Imaging performance characterization

A Z-scan OCT sensitivity measurement was performed to determine the intensity distribution as a function of distance from the probe distal end surface: a reflective mirror placed

#258710 Received 2 Feb 2016; revised 29 Feb 2016; accepted 1 Mar 2016; published 4 Mar 2016

orthogonal to the output beam propagation direction was translated across the axial field of view of the probe, and the sensitivity was recorded at different depths.

In order to characterize the optical performance of the system and fiber probe, we made a tissue scattering phantom comprised of 0.5% 2-μm diameter polystyrene microspheres (Polysciences, Inc. PA, USA) mixed with 1% agar (SIGMA-ALDRICH, MO, USA). A motorized stage translated the probe to acquire B-scan images of the phantom.

3. Results

To demonstrate this new optical configuration for flexible catheter or endoscope based scanning OCT applications, we designed a self-imaging wavefront division fiber optic probe to be 500 μm in diameter and have a rigid length of approximately 4 mm. Figure 2(a) is a photograph of the assembled self-imaging wavefront division fiber optic probe prototype, and Fig. 2(b) shows the ring pattern of the beam emitted from the probe in the far field, demonstrating its multi-mode annular propagation pattern. The single-pass loss of the probe was measured to be 1.5 dB over 650-950 nm spectrum and the backreflection was <-47 dB neglecting the common-path reference reflectance and the system's fiber port collimator's backreflection.

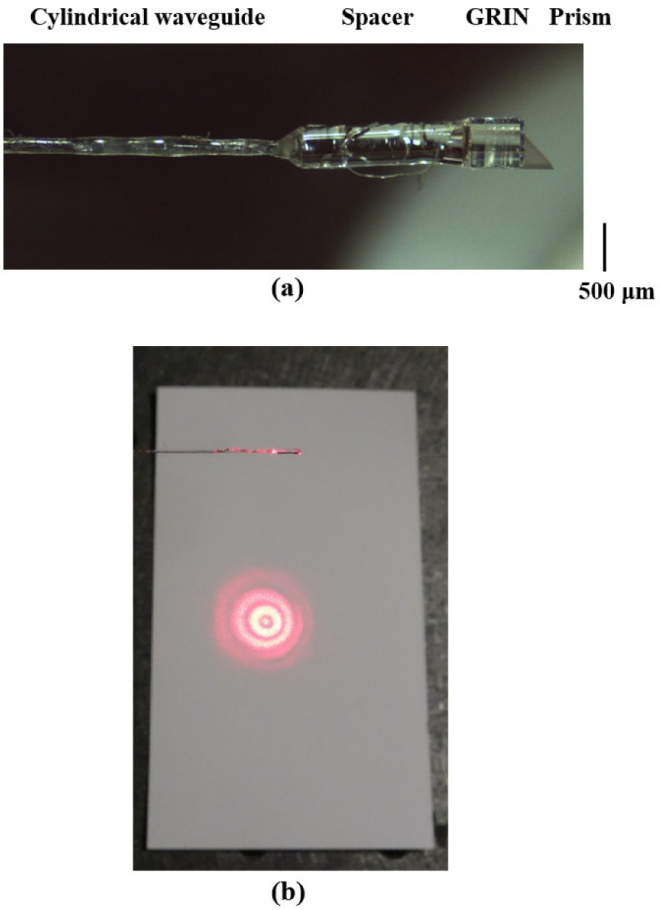

Fig. 2. (a) Photograph of the common-path self-imaging wavefront division fiber optic probe. (b) Transmitted far field ring pattern on the plane normal to the beam propagation direction.

#258710 Received 2 Feb 2016; revised 29 Feb 2016; accepted 1 Mar 2016; published 4 Mar 2016

3.1 Z-scan sensitivity measurement

With an approximately 20 mW total probe intensity output, the Z-scan sensitivity across the 1 mm extended focus ranged from 80 dB to 88 dB. The axial resolution was measured to be 2 μm (FWHM of axial PSF) in air over the entire depth range. In order to compare our measurements with the simulated depth intensity profile, the system's sensitivity roll-off was characterized by an external interferometer; the actual fiber probe output intensity distribution as a function of depth was estimated as the measured Z-scan sensitivity with spectrometer sensitivity roll-off compensated. Figure 3(a) depicts the simulated intensity-depth profile in air, Fig. 3(b) is the measured spectrometer sensitivity roll-off, Fig. 3(c) is fiber probe Z-scan sensitivity measurement, and Fig. 3(d) is the Z-scan sensitivity measurement compensated by the spectrometer roll-off values. As can be seen in Fig. 3(d), the corrected, experimentally determined Z-scan measurement is in reasonable approximation to the simulation (Fig. 3(a)). The difference between the simulated profile (Fig. 3(a)) and the actual measurement profile (Fig. 3(d)) may be explained by 1) errors in the fiber probe's fabrication process relative to the parameters used in the simulation; 2) chromatic aberration introduced by optics; and/or 3) differences in collection efficiencies between modes.

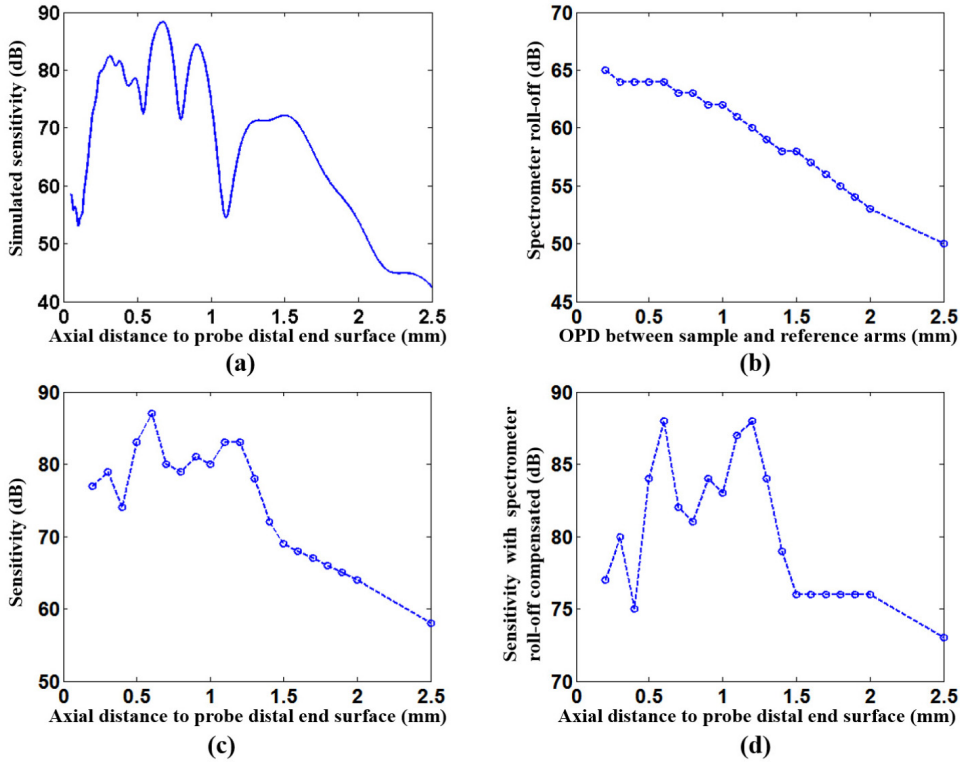

Fig. 3. (a) Simulated intensity vs. depth in air where the sensitivity noise level is set to be consistent with measurement result. (b) OCT spectrometer sensitivity roll-off characterized by an external interferometer. OPD: optical pathlength difference. (c) Self-imaging wavefront division fiber optic probe Z-scan measurement. (d) Z-scan measurement compensated by sensitivity roll-off shown in (b).

3.2 Scattering tissue phantom image

Figure 4 shows μOCT images of the phantom obtained with the probe shown in Fig. 2(a). The DOF enhancement can be clearly seen, with bright and sharply defined particles are seen over an axial field of view that is greater than 1 mm. The consistency of the probe's sensitivity

#258710 Received 2 Feb 2016; revised 29 Feb 2016; accepted 1 Mar 2016; published 4 Mar 2016

over its multiple foci also results in highly uniform images; the overlap of focused adjacent modes minimizes the perception of discontinuity between focal zones. Since a broad spectrum is used for imaging, chromatic aberration caused by the optics results in a certain degradation on the axial and lateral resolutions, but the effect of the chromatic focal shift also mitigates the image discontinuity associated with the intensity gaps found between focused modes (Fig. 1(c)).

By quantitatively analyzing the axial PSF (Fig. 5(a)) at multiple depths (intensity in linear scale), the FWHM of axial PSF was found to be 2 μm throughout the image, indicating a nearly dispersion-free interferometric system due to the common-path configuration. The axial resolution is slightly degraded compared with theoretical value due to chromatic aberration of the optics. The measured FWHM of lateral PSF is plotted as a function of depth in Fig. 5(b). The lateral PSFs at depths of interest are also presented, showing no significant side-lobe artifacts. The finest FWHM of the in-focus lateral PSF was measured to be 3.0 μm, and the FWHM was maintained within 4.2 μm for most of the lateral PSFs throughout a 1 mm depth range. Compared with a conventional Gaussian beam, a 3.0-μm PSF FWHM corresponding to a 2.5-μm beam waist, would generate a DOF of 50 μm (twice the Rayleigh range) at 800 nm wavelength. These measurements indicate that this self-imaging wavefront division fiber optic probe attained a 20-fold DOF extension.

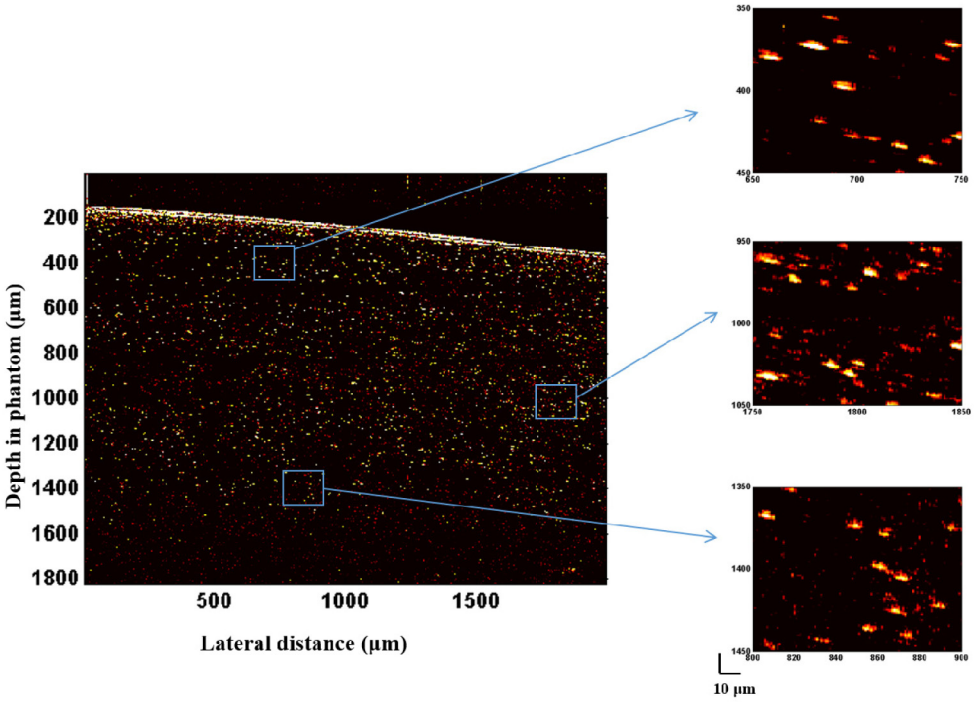

Fig. 4. μOCT B-scan phantom image acquired by the self-imaging wavefront division fiber optic probe. Three insets on the right are zoomed images at different depths indicating a well maintained lateral resolution over more than a 1 mm depth range. Vertical and horizontal axes are in μm units. 10 μm scale bars on the lower right applies to the insets.

#258710 Received 2 Feb 2016; revised 29 Feb 2016; accepted 1 Mar 2016; published 4 Mar 2016

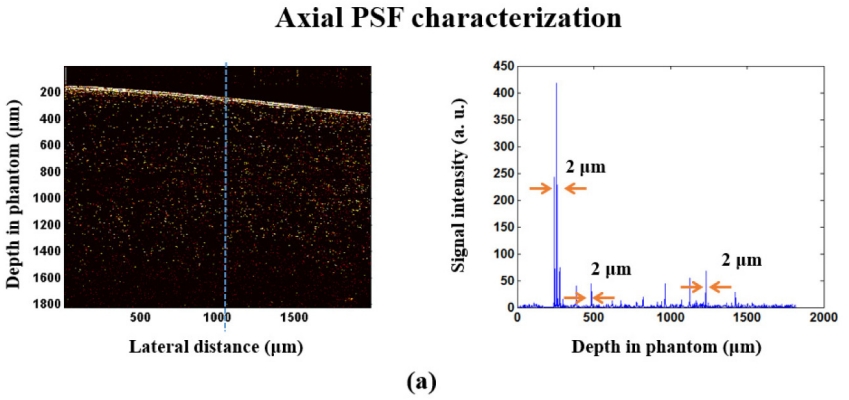

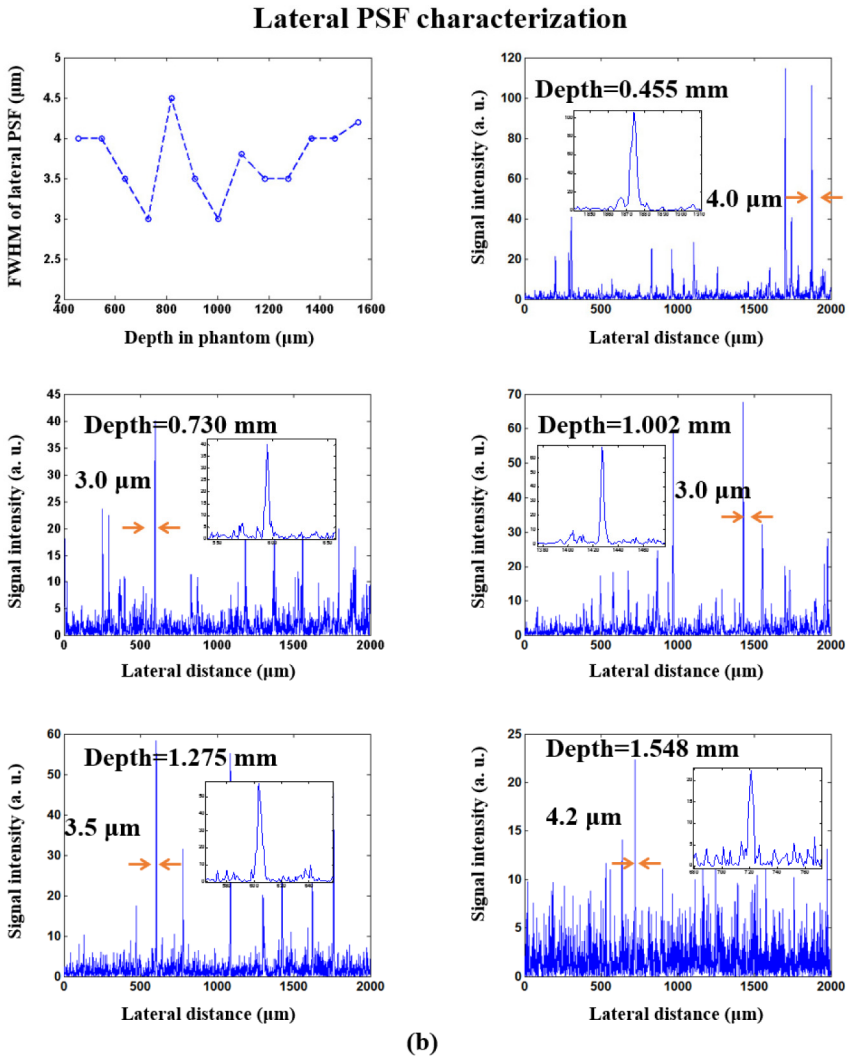

Fig. 5. PSF characterization. (a) A μOCT A-scan (right) taken from the dotted line in the phantom image (left), demonstrating a 2-μm axial PSF FWHM over the entire 1 mm depth range. (b) Measured FWHM of lateral PSF vs. depth in phantom, indicating that the FWHM was maintained within 4.2 μm for most of the lateral PSFs across the entire 1 mm depth range.

#258710 Received 2 Feb 2016; revised 29 Feb 2016; accepted 1 Mar 2016; published 4 Mar 2016

4. Discussion

4.1 Multi-focus OCT sample arm

The self-imaging wavefront division fiber optic probe demonstrated here applies a single-beam multi-focus scheme to significantly extend the DOF. For a conventional multi-focus technique, multiple Gaussian beams are relayed to extend the DOF, thus the DOF is simply proportional to the number of beams deployed. For this self-imaging wavefront division technique, the DOF for each high order mode is longer than that of conventional Gaussian beams and therefore fewer foci are required to achieve a comparable extension of the DOF.

4.2 Lateral PSF artifacts

The multi-mode propagation scheme introduces a ring pattern on the plane normal to the beam propagation direction (Fig. 2(b)). At each mode's focal plane, other modes present as a potential side-lobe or out-of-focus artifacts that could blur the in-focus mode. But since the SMF core spatially filters the backscattered light, off-axis scattering centers are strongly attenuated [20] and no significant side-lobe artifacts are observed as shown in Fig. 4 and Fig. 5(b).

4.3 Sensitivity considerations

Since the cylindrical waveguide imposes an additional aperture for the lens system and the high order modes of our probe are similar to Bessel optics that have a limited detection spatial frequency bandwidth, a certain signal loss is expected. At 20 mW supercontinuum laser output power, and a 38 kHz A-scan rate, and deducting signal losses due to those in the μOCT imaging system itself, the μOCT sensitivity was expected to be approximately 100 dB if conventional Gaussian optics were utilized in the sample arm. According to the simulations, the cylindrical waveguide divides energy into multiple propagation modes, 15% energy for the 0th order mode, 60% energy for 1st order mode, and 25% for 2nd and even higher order modes, therefore, ideally, we expect 0th order mode sensitivity 92 dB, 1st order mode sensitivity 98 dB, and 94 dB for higher order modes. However, our measured sensitivity obtained by Z-scanning (Fig. 3(d)) ranged between 80 dB and 88 dB over the axial field of view. We therefore estimate that there is an overall 5-10 dB signal loss that can be attributed to the implementation of this wavefront division configuration. Improvements in image sensitivity can be accomplished by optimizing system SNR [21, 22] or by increasing the source power further within tissue exposure limits.

4.4 Multi-mode propagation scheme

A well-managed optical pathlength difference between modes and an effective attenuation of mode cross-coupling are required for this technique to be effective as demonstrated. The single-pass optical pathlength differences introduced by the cylindrical waveguide between 0th order and 1st order modes, and 1st order and 2nd order modes were calculated to be on the same order of system's axial resolution (a few microns). As a result, no perceptible gaps were observed in the image. The possibility of cross-coupling the modes from the backscattered light is greatly reduced owing to the confocal pinhole effect (single mode spatial filtering) of the SMF core since different modes are designed to come to a focus at different depth regions.

4.5 Distal end circumferential scan

For endoscope or catheter imaging, circumferential scan and axial pull-back is usually performed to acquire *in-vivo* 3D images. As μOCT provides lateral resolution that is one order of magnitude better than that of conventional OCT systems, a scanning mechanism with higher precision and stability is required. Recently, a high-speed distal end motor for intravascular OCT imaging has been demonstrated to improve the circumferential scan stability and boost the scanning speed [23], which also may be helpful for catheter-based μOCT using this extended DOF probe.

#258710 Received 2 Feb 2016; revised 29 Feb 2016; accepted 1 Mar 2016; published 4 Mar 2016

5. Conclusion

In summary, we have designed and fabricated a single-fiber, common-path self-imaging wavefront division probe with 500-μm diameter optics and a 4-mm rigid length that provides a 20-fold DOF extension. B-scan image of a scattering phantom indicates that the fiber optic probe can significantly extend the DOF of OCT system, maintaining high quality, high-resolution (approximately 3 μm lateral and 2 μm axial resolutions) imaging throughout an axial depth of field of greater than 1 mm. This extended DOF design addresses the most critical barrier to high-resolution imaging using scanning OCT probes inside the body. Our probe design is also compact and easy to fabricate, which will facilitate translation to the clinic.

Acknowledgments

The authors thank Dr. Joseph Gardecki for his help in OCT imaging and experimental sample preparation. This study is supported by NIH grant R01HL076398.

Dr. Tearney receives sponsored research funding from Ardea Biosciences and Canon Inc. Massachusetts General Hospital has a licensing arrangement with Terumo Corporation. Dr. Tearney has the rights to receive royalties from this licensing arrangement. Dr. Tearney also receives royalties from MIT.

#258710 Received 2 Feb 2016; revised 29 Feb 2016; accepted 1 Mar 2016; published 4 Mar 2016